Spectroscopic Study of Shock-Induced Decomposition in Ammonium Perchlorate Single Crystals

Y. A. Gruzdkov, J. M. Winey, and Y. M. Gupta*

Institute for Shock Physics and Department of Physics, Washington State University, Pullman, Washington 99164-2816

Received: December 18, 2007; In Final Form: February 7, 2008

Time-resolved Raman scattering measurements were performed on ammonium perchlorate (AP) single crystals under stepwise shock loading. For particular temperature and pressure conditions, the intensity of the Raman spectra in shocked AP decayed exponentially with time. This decay is attributed to shock-induced chemical decomposition in AP. A series of shock experiments, reaching peak stresses from 10−18 GPa, demonstrated that higher stresses inhibit decomposition while higher temperatures promote it. No orientation dependence was found when AP crystals were shocked normal to the (210) and (001) crystallographic planes. VISAR (velocity interferometer system for any reflector) particle velocity measurements and time-resolved optical extinction measurements carried out to verify these observations are consistent with the Raman data. The combined kinetic and spectroscopic results are consistent with a proton-transfer reaction as the first decomposition step in shocked AP.

I. Introduction

Ammonium perchlorate (AP) has long been of chemical interest because of its wide use in propellants. Understanding shock-induced chemical decomposition of AP is important for many applications and for safety in shipping and storage. Because of its practical importance, the physical and chemical properties, decomposition, and combustion of AP have been widely studied. Good reviews of these subjects can be found in refs 1−3.

More recently, work has focused on the response of AP to shock wave loading. In wave propagation experiments, the mechanical response of AP single crystals was examined for shock loading to 6 GPa.[4] Using these results, along with temperatures determined from Raman spectroscopy measurements for shocked AP, a thermo-mechanical material model was developed for unreacted AP single crystals.[5] Also, the phase diagram of AP was examined under static high pressure.[6] Despite these advances, determination of the mechanism for chemical decomposition in shocked AP remains an important need. For safety and efficiency in applications, it is also important to determine the sensitivity of AP to external stimuli and to determine the effects of pressure and temperature on the decomposition threshold and reaction rate.

To address these needs, a combination of continuum measurements (stress, particle velocity) and time-resolved spectroscopic (electronic, vibrational) techniques must be employed.[7] Therefore, in the work presented here, we utilized previous developments regarding time-resolved vibrational and electronic spectroscopy of shocked energetic materials[8−11] to examine AP single crystals. Time-resolved Raman spectroscopy was used as the primary tool because it can serve as a direct in situ probe sensitive to both chemical and structural changes in AP.[12] Our Raman experiments were supplemented with optical extinction and VISAR (velocity interferometer system for any reflector)[13] particle velocity measurements. As a result, the data could be analyzed in a self-consistent manner. The experiments were carried out under well-characterized planar shock wave loading, which eliminated the ambiguities of complex loading conditions and/or indirect measurements.[14,15]

The objectives of this work were (1) to observe evidence for chemical reaction under shock loading, (2) to evaluate the effects of stress, temperature, and crystal orientation on the reaction rate, and (3) to assess the applicability of previously proposed mechanistic models for decomposition[1−3] to shock wave loading conditions.

The remainder of this paper is organized as follows: In section II, we describe the experimental methods used in this work. The experimental results are presented in section III. In section IV, we discuss our main findings and a summary is given in section V.

II. Experimental Method

A. Crystal Preparation. All single crystals used in this work were supplied by Dr. T. L. Boggs of Naval Air Warfare Center, China Lake, CA. The crystals were cleaved parallel to the (210) or (001) faces to yield thin slides of approximately 12 mm width and 2 mm thickness. The slides were processed according to the following procedure: Rough grinding was done wet on 30 μm aluminum oxide lapping sheets (Fiber Optics Center, MA), using a nearly saturated solution of AP in water as a lubricant. Fine grinding was done dry on 9 μm sheets. During the grinding process, the sample thickness and parallelism were checked periodically using a micrometer and an optical flat. The final optical finish was produced in two steps using 1 μm and 0.3 μm aluminum oxide powders suspended in oil (Automet Lapping Oil, Buehler). The polishing was done on an adhesive backed cloth (Chemomet Cloth, Buehler) attached to a glass plate. All grinding and polishing was carried out under a laminar-flow clean hood. The procedure resulted in an optically clear sample approximately 450 μm thick. Typically, the

* Corresponding author.

10.1021/jp711872u CCC: $40.75
Published on Web 03/21/2008

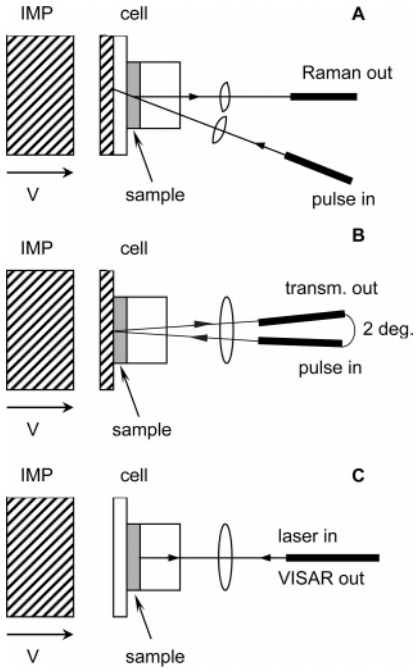

Figure 1. Target assemblies for (A) Raman, (B) double-pass light extinction, and (C) VISAR measurements. Shock waves are launched by impact between an impactor (IMP) and the front anvil of the sample cell. Sample thickness (shaded area), typically 0.4 mm, is exaggerated in the drawing. A pulse of light either from a laser (Raman, VISAR) or from a Xe flashlamp (extinction) is delivered through an optical fiber positioned behind the cell. The scattered (Raman) or reflected (extinction, VISAR) light is then gathered into the collection fiber and transmitted to the detection equipment. In the case of VISAR, a single fiber is used for both light delivery and collection.

thickness across the sample was uniform to better than 1% and the surfaces were flat to approximately 5 wavelengths of visible light.

B. Overall Configuration. Shock waves were generated by impact between an impactor, mounted on a projectile, and the front anvil of the sample cell as shown in Figure 1(A−C). The projectile was accelerated to velocities as high as 1.2 km/s using a single stage gas gun.[16] For velocities higher than 1.2 km/s, a 20 mm powder gun was used.[17] After traversing the front anvil, the shock wave reverberated between the cell anvils bringing the AP to the final stress and temperature via a stepwise loading process. The final stress was maintained until release waves arrived from the edges of the AP crystal at approximately 800 ns after the shock entered the sample.

Stress and temperature histories for the sample in each experiment were calculated using a one-dimensional finite-difference wave code and the material model for AP developed previously.[5] Because the impact velocity and the shock response of the impactor and cell anvils are well-known,[18−21] the calculated final stress is accurate to within 1−2%. Temperature measurements in shocked AP, using Raman scattering, showed that the calculated temperatures are accurate to better than 10%.[5]

The instrumental configuration to obtain time-resolved Raman scattering data in this work was similar to that used previously.[9] Excitation light from a pulsed dye laser (Cynosure LFDL-8E, 3.5 μs pulse duration) operating at 514.5 nm was delivered to the sample using an optical fiber. Raman scattered light from the sample was fiber-coupled to a spectrometer (HoloSpec f/1.8i spectrometer, Kaiser Optical Systems) for spectral dispersion and passed to a streak camera (Imacon 500, Hadland Photonics) for time dispersion. The resulting signal was collected using an image intensifier and a CCD detector.

The instrumental configuration (fiber-coupled spectrometer/streak camera/CCD) used to obtain time-resolved optical transmission data was the same as that utilized previously.[10] However, in the work presented here, a double pass transmission geometry (see Figure 1B) was used, necessitating changes in the target assembly as described below.

The interferometer used for VISAR particle velocity measurements was of a conventional design[13] and is described in detail elsewhere.[22] An Ar−ion laser operating in a single mode at 514.5 nm, with a line width of 15−20 MHz, provided the incident light.

C. Target Design. To allow for uniform loading throughout the sample, the thin AP sample was sandwiched between two anvils resulting in a stepwise loading process. Lateral dimensions allowed for at least 800 ns of recording time before edge release waves arrived in the probed central region of the crystal. A summary of various anvil combinations employed is given in Table 1. For Raman experiments, liquid nonane (anhydrous, 99+%, Aldrich Chemical) was used to fill gaps between the sample and anvils. For optical extinction and VISAR experiments, the sample was bonded to the anvils using UV-grade epoxy (Epo-Tek 301, Epoxy Technology). A typical gap or bond was less than 5 μm thick. In a separate set of experiments, we verified that both nonane and epoxy remain optically transparent under the loading conditions of interest.

The Raman target design used in this work was similar to that used previously.[9] In several Raman experiments (R1-R3, R8), OFHC copper impactors and buffers were used instead of sapphire (see Figure 1A). The internal surface of the Cu buffer was polished to a mirror finish to reflect the intense laser pulse impinging on the sample. Care was taken to avoid laser damage to the polished copper surface.

Figure 1B shows a schematic diagram of the target assembly for extinction measurements. The highly polished surface of the stainless steel (SS304) buffer served as a mirror to allow the probe light to pass twice through the sample before it was collected for detection. Under shock, a SS304 polished surface, unlike many other materials, is known to retain much of its reflectivity.[23] An aperture attached to the back LiF window limited the beam diameter to 2 mm. The excitation and collection fibers were arranged into a fiber bundle behind the cell. The tip of the excitation fiber was imaged onto the tip of the collection fiber by adjusting the angle between the two fibers. The resulting angle was approximately 2 degrees; the distance between the tips was 1.5 mm.

To perform VISAR particle velocity measurements, the LiF surface adjacent to the backside of the sample (see Figure 1C) was vapor-deposited with an aluminum film approximately 200 nm thick. A single optical fiber delivered the laser light to the target and transported the Doppler shifted light back to the interferometer.

III. Results and Analysis

Experimental details pertinent to the time-resolved Raman and extinction experiments and the VISAR experiments are summarized in Table 1. A total of fifteen experiments is presented: nine Raman experiments, four extinction experiments, and two VISAR experiments.

A. Raman Scattering. The Raman spectrum of AP can be found in the literature, where reliable peak assignments have been made previously.[12,24] A summary of the AP Raman modes observable in this work is given in Table 2. The NH_4^+ antisymmetric stretching mode (T_2 symmetry) at 3350 cm^{-1} and

TABLE 1: Experiment Results

experiment #	crystal orientation	sample thickness (μm)	long. stress (GPa)	calculated temperature[a] (K)	impact velocity (km/s)	impact configuration: impactor; front anvil; back anvil
			Raman Experiments			
R1 (97−007)	(210)	450	10.5	527	0.932	Cu; Cu/LiF; LiF
R2 (97−002)	(210)	485	13.4	599	1.154	Cu; Cu/LiF; LiF
R3 (96−045)	(001)	475	15.3	577	0.879	Cu; Cu/LiF; sapphire
R4 (96−033)	(210)	475	15.7	585	0.861	sapphire; LiF; sapphire
R5 (97−012)	(210)	400	16.3	595	0.886	sapphire; LiF; sapphire
R6 (98−011)[b]	(210)	485	16.5	697	0.895	sapphire; LiF; sapphire
R7 (97−017)	(001)	405	16.7	602	0.906	sapphire; LiF; sapphire
R8 (98−744)	(210)	480	17.7	714	1.460	Cu; Cu/LiF; LiF
R9 (98−018)[c]	(210)	455	18.1	758	0.974	sapphire; LiF; sapphire
			Optical Extinction Experiments			
A1 (97−009)	(210)	380	12.4	562	1.072	SS304; SS304; LiF
A2 (97−008)[d]		N/A	13.1		1.125	SS304; SS304; LiF
A3 (98−759)[d]		N/A	17.5		1.445	SS304; SS304; LiF
A4 (98−760)	(210)	440	18.0	688	1.475	SS304; SS304; LiF
			VISAR Experiments			
V1 (98−750)	(001)	485	17.2	690	1.419	Cu; LiF; LiF
V2 (98−751)	(210)	470	17.5	701	1.444	Cu; LiF; LiF

[a] Temperature calculation using the material model for AP developed in ref 5. [b] Heated to 373 K prior to experiment. [c] Heated to 403 K prior to experiment. [d] Reference experiments; contained no sample. The back window was directly attached to the SS304 buffer.

TABLE 2: AP Raman Modes[a]

	freq./cm^{-1}	sym.	assignment
ν_1	3209	A_1	NH_4^+ sym. stretch
ν_{2-4}	1129	T_2	ClO_4^- anti-sym. stretch
ν_{2-4}	1104	T_2	ClO_4^- anti-sym. stretch
ν_{2-4}	1060	T_2	ClO_4^- anti-sym. stretch
ν_5	933	A_1	ClO_4^- sym. stretch
ν_6	627	T_2	ClO_4^- bend
ν_7	461	E	ClO_4^- bend

[a] Taken from ref 12.

NH_4^+ bending modes at 1420 cm^{-1} (E symmetry) and at 1680 cm^{-1} (T_2 symmetry) are weak[12,24] and were not resolvable in our spectra.

Figure 2 shows representative Raman spectra of AP acquired with two different instruments. Spectrum A was acquired using a high resolution (1 cm^{-1}) CW Raman instrument. As can be seen, the fine details of the peak shapes could be resolved. For instance, the Fermi resonance-enhanced first overtone of ν_7 is clearly discernible as a low energy shoulder on the ν_5 peak. Spectrum B was acquired during a single laser pulse using the system for time-resolved measurements. Because this system is designed to provide both broad spectral coverage (>4000 cm^{-1}) and a strong Raman signal, it limits the spectral resolution to approximately 50 cm^{-1}. At this resolution, the recorded widths of all observed peaks are determined solely by the instrument profile and information about the individual line shapes is lost. Hence, our measurements contain no information regarding the effects of shock compression on peak widths. However, the peak positions could be determined to within ± 3 cm^{-1}.

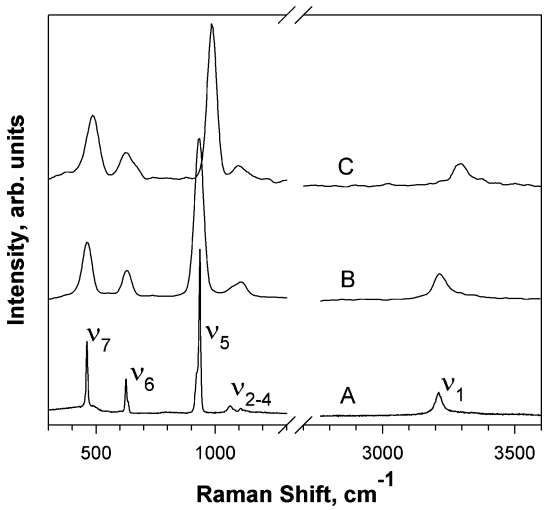

Figure 2. Raman spectra of AP. Trace A, at ambient pressure, acquisition time 1 min with a CW Ar-ion laser; trace B, at ambient pressure, acquisition time 1 μs with a pulsed dye laser; trace C, shocked to 15.7 GPa [(210) orientation], acquisition time 0.5 μs using the same instrumentation as B. The spectra are vertically offset for clarity.

Spectrum C of Figure 2 was acquired from AP shocked to 15.7 GPa. Under shock compression, all peaks shifted to higher vibrational frequency. The measured stress-induced shifts of ν_1, ν_5, and ν_6 are plotted in Figure 3 (the shift of ν_7 could not be determined accurately because of strong interference from elastically scattered laser light). Between 10 and 18 GPa, the shifts appear to increase approximately linearly with stress. The frequency-stress coefficients determined from Figure 3 are 4.53, 3.55, and 2.55 cm^{-1}/GPa for ν_1, ν_5, and ν_6, respectively. Extrapolation of the linear fits to zero stress shows that the frequencies must shift nonlinearly over a broader (0 − 18 GPa) stress interval. The majority of our experiments were performed with the (210) orientation. However, two experiments were carried out with the (001) orientation at 15.3 and 16.7 GPa. As can be seen from Figure 3, no orientation dependence was observed at these stresses.

Figure 4 shows time-resolved Raman spectra for the (210) orientation of AP shocked to 13.4 GPa (expt R2). As evident from the data, the intensity of the Raman signal gradually decreases after the shock wave enters the sample. A careful examination of possible experimental artifacts, such as window failures, sample translation, etc., showed that this decrease in Raman signal was indeed due to shock-induced processes in the sample. To varying extent, it was observed in all of our Raman experiments. As will be demonstrated below, this effect can be attributed to a chemical reaction that consumes the AP, thus decreasing the Raman signal. The decay rate of the Raman signal may therefore be interpreted as the AP decomposition rate. Given this interpretation, one can examine the effects of

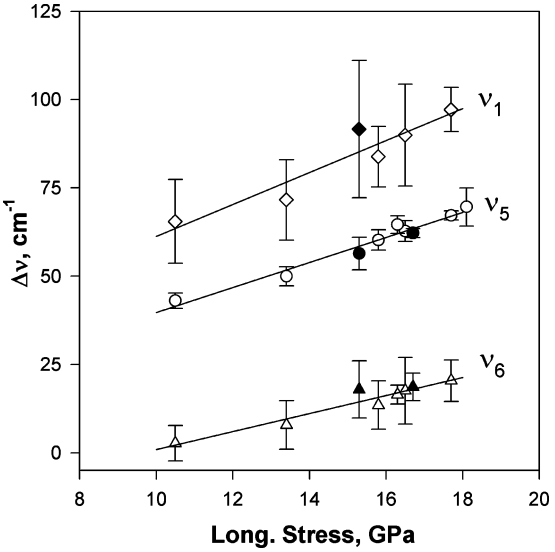

Figure 3. Shock-induced change in Raman frequency versus final stress in AP: triangles, ClO_4^- bend (627 cm^{-1}); circles, ClO_4^- symmetric stretch (933 cm^{-1}); diamonds, NH_4^+ symmetric stretch (3209 cm^{-1}). Empty and solid symbols represent the (210) and (001) orientations, respectively. Solid lines depict linear regressions. The calculated slopes are 2.55, 3.55, and 4.53 cm^{-1}/GPa for the 627 cm^{-1}, 933 cm^{-1}, and 3209 cm^{-1} modes, respectively. The error bars represent average spectrum-to-spectrum variations in the position of the peak.

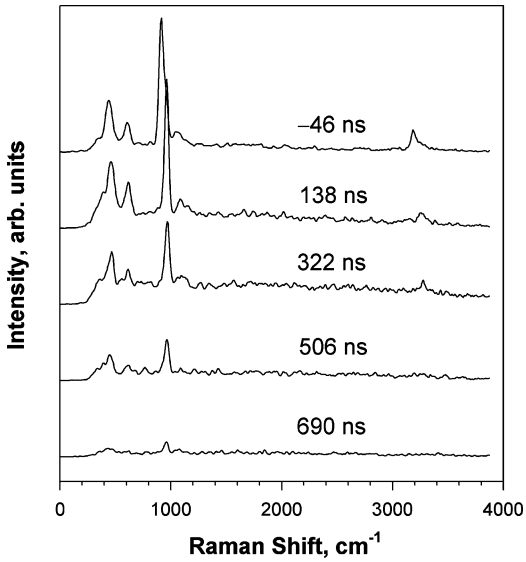

Figure 4. Time-resolved Raman spectra for the (210) orientation of AP shocked to 13.4 GPa (expt R2). The spectra were acquired with 46 ns time resolution; only the spectra at −46, 138, 322, 506, and 690 ns are shown. Time is relative to when the shock wave entered the sample. The spectra are vertically offset for clarity.

pressure and temperature on the decomposition process. In shock loading processes, it is difficult to uncouple these two variables. However, reverberation experiments, unlike single shock experiments, allow different thermodynamic states to be accessed by varying the anvil materials. In our Raman experiments, we utilized this approach to decouple temperature and pressure, relying on the AP material model for temperature calculations.[5]

Figure 5 shows the area under the peak of ν_5 as a function of time in three experiments. Signal decay rates were determined by fitting the data with exponential functions; the fits are shown as the solid lines in the figure. In expts R5, R6, and R2, the final stress (temperature) states were calculated to be 16.3 GPa (595 K), 16.5 GPa (697 K), and 13.4 GPa (599 K), respectively. Comparing the results of expts R5 and R6 reveals the expected

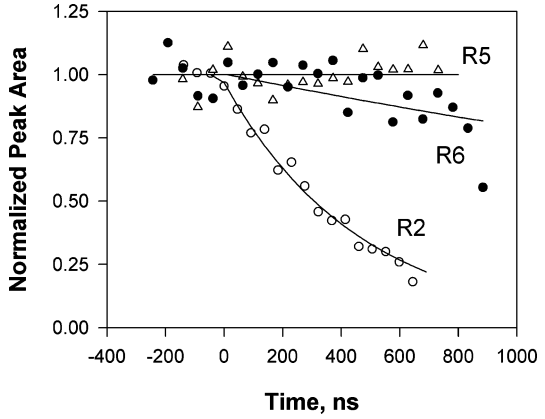

Figure 5. Normalized area under the peak for the ClO_4^- symmetric stretching mode (933 cm^{-1}) versus time. Results for expt R5 (16.3 GPa/595 K), expt R6 (16.5 GPa/697 K), and expt R2 (13.4 GPa/599 K) are shown. Solid lines represent the first-order kinetic fits.

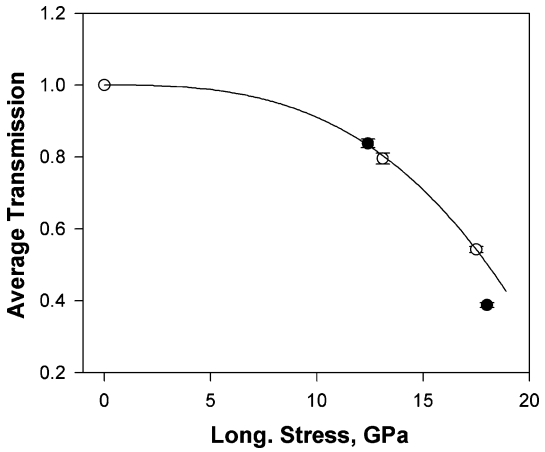

Figure 6. Average transmission through the cell as a function of final stress. Averaging intervals for time and wavelength are 300−600 ns and 400−600 nm, respectively; time is relative to when the shock wave reached the reflecting surface. Empty dots represent reference expts A2 and A3, in which the cell contained no sample, and data at ambient pressure. The curve is a third-order polynomial fit to the reference data. Solid dots represent expts A1 and A4 in which an AP crystal was shocked normal to the (210) plane.

result that an increase in temperature speeds up the decomposition at 16 GPa. By comparing expts R5 and R2, one finds that at about 600 K the increase in stress from 13 to 16 GPa retards the decomposition. This type of behavior indicates that the activation volume of the rate controlling reaction is positive.

B. Double-Pass Optical Extinction. The optical extinction experiments were performed to verify that the decreases in the Raman signal described above were not caused by light attenuation because of absorption or scattering.

An important difference between the double-pass extinction configuration employed here and the configuration utilized previously[10] is that the metal buffer serving as a mirror (see Figure 1B) is subjected to a shock wave. Hence, reflectivity changes due to shock loading must be accounted for in data reduction. To measure these changes, reference experiments (with no sample in the cell) were performed for each double-pass AP experiment (see Table 1). The results of the reference experiments are plotted against stress in Figure 6. The loss of transmission with stress is assigned to reflectivity loss in the metal buffer.

Because of unavoidable, but small, variations in the projectile velocity, the final stresses in reference and AP experiments were

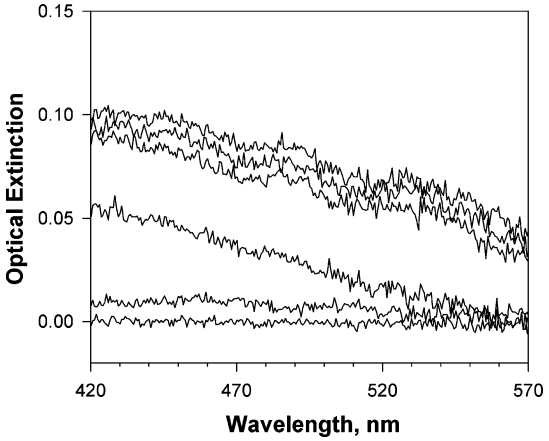

Figure 7. Time-resolved extinction spectra of AP shocked to 18.0 GPa (expt A4). The spectra were acquired with 50 ns resolution; only the spectra at −200, 0, 200, 400, 600, and 800 ns are shown. Time is relative to when the shock wave entered the sample.

slightly different. To correct for these differences, a third-order polynomial, $F_3(\sigma)$, was fitted to the reference data, as shown in Figure 6. Using this polynomial, we calculated correction factors, $\Omega = F_3(\sigma_{AP})/F_3(\sigma_{ref})$, for each pair of experiments, where σ_{AP} and σ_{ref} are the final stresses in the AP and reference experiments, respectively. Extinction, A, was then calculated from the streak camera data using the following formula:

$$A(\lambda,t) = -\log \{[I_{AP}(\lambda,t) - I_b(\lambda,t)]/[\Omega\, I_{ref}(\lambda,t) - I_b(\lambda,t)]\}$$

where $I_{AP}(\lambda,t)$ and $I_{ref}(\lambda,t)$ are the transmitted signals as a function of wavelength and time in the AP and reference experiments, respectively, and $I_b(\lambda,t)$ is the background signal acquired with the streak camera shutter closed.

No extinction changes originating in the AP sample were detected in expt A1. This observation is illustrated by the point corresponding to this experiment in Figure 6, which falls on the reference curve. However, extinction changes were observed in expt A4, with the extinction spectra shown in Figure 7. As can be seen, the attenuation of transmitted light is small, not exceeding 0.07 for $\lambda > 514$ nm. This value would correspond to no more than 15% attenuation of the Raman signal. The experimental parameters of expts A1 and A4 are very close to those in Raman expts R2 and R8, respectively. In each of those experiments, the Raman signal decreased by at least 70% within 700 ns. Such a large decrease could not be accounted for by the observed light extinction. Therefore, the most plausible explanation is a chemical reaction.

C. VISAR. If the changes in the Raman signal are indeed caused by the decomposition of AP, then the extent of reaction must be significant. Large extents of reaction manifest themselves in continuum measurements as changes in stress and particle velocity due to energy release from the reaction. Therefore, by performing VISAR particle velocity measurements, we could independently verify our interpretation of the Raman signal decay as due to a chemical reaction.

The configuration chosen was essentially the same as in the Raman experiments (see Table 1 and Figure 1C). The measured particle velocity histories from expts V1 and V2 are shown in Figure 8. Similar results are observed for the (210) and (001) orientations. In both cases, we observed a noticeable acceleration of the AP/LiF interface from approximately 600 ns to the arrival of the release waves at 800 ns. This behavior is characteristic of pressure build-up in the sample because of chemical reactions. If the extent of reaction was small or if the AP did not react, the particle velocity records would be expected to follow the computed profiles for unreacted AP (Figure 8). In fact, a good match between the particle velocity histories and the unreacted profiles was found at lower stresses where the extent of reaction, as inferred from the Raman data, was small. Thus, the VISAR data corroborate the interpretation of the Raman data given above.

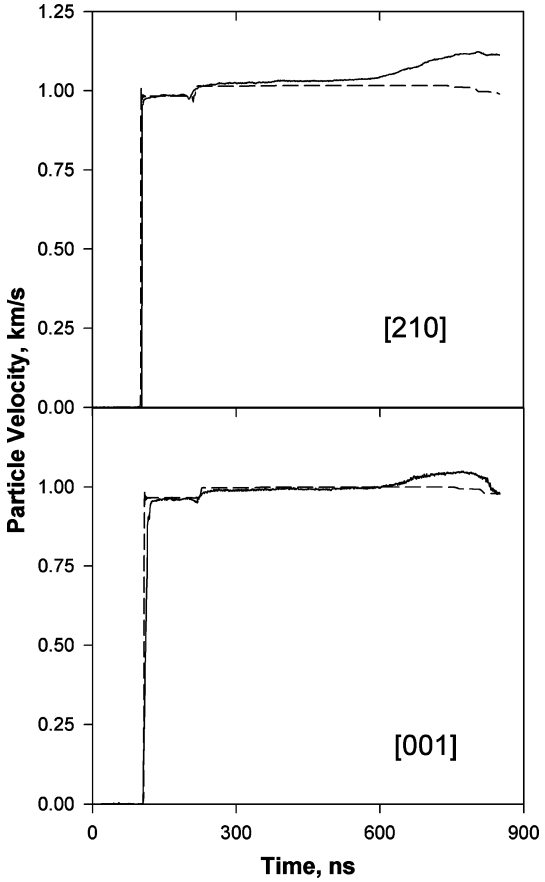

Figure 8. Measured and computed AP-LiF interfacial velocity histories for the two VISAR experiments: (210) orientation, expt V2; (001) orientation, expt V1. The solid lines are the data and the dashed lines are numerical simulations using the unreacted AP model (ref 5). Time is relative to when the shock wave entered the sample. The estimated arrival of the edge release waves occurs at 800 ns.

IV. Discussion of Results

The decomposition and combustion of AP were studied extensively in the 1960s.[1−3] The processes are very complex because of the presence of four elements and the full range of oxidation states utilized by nitrogen and chlorine. In excess of 1000 reactions may be involved in the decomposition before the final products are formed.[25] Despite the complexity, under a variety of conditions examined, the common initial step was found to be one of proton transfer:

$$NH_4^+ ClO_4^- \rightarrow NH_3 + HClO_4 \qquad (1)$$

Subsequent reaction is then dominated by conventional perchloric acid chemistry.[2] Below, we analyze our experimental observations to assess the applicability of reaction 1 to the conditions of shock compression.

Ionic reactions, particularly where there is creation or annihilation of charge in the transition state, are strongly affected by pressure.[26] In general, charge destruction reactions, like reaction 1, display positive activation volumes, $\Delta V^{\neq}$, on the

order of 10−20 cm^3/mol.[27] Given the results shown in Figure 5 (expts R2 and R5), we can estimate the activation volume for decomposition under shock compression and compare it with the value expected for reaction 1. Since there is virtually no signal decay observed in expt R5 within the experimental error, one can only obtain the upper bound of the rate constant, k. The constant appears to be less than 5×10^4 s^{-1}. By fitting the data of expt R2 with first-order kinetics, one finds $k = 2.1 \times 10^6$ s^{-1}. Then, using these values and the definition of activation volume, we estimate $\Delta V^{\neq} \geq 6.4$ cm^3/mol.[28] This value is consistent with reaction 1. A similar estimate can be obtained for the activation energy, E_0, from expts R5 and R6. We find that $E_0 \geq 12$ kcal/mol, which is also consistent with the value of 20−30 kcal/mol reported for reaction 1 in the literature.[1,29]

Furthermore, the overall spectroscopic observations are consistent with reaction 1 as well. The immediate products of reaction 1, ammonia and perchloric acid, do not absorb light in the visible. Possible absorbing species such as NO_2Cl, NO_2, NOCl, and so forth are not expected to form until very far into the reaction sequence.[2] Therefore, the lack of absorbance observed in the 400−600 nm region is consistent with reaction 1. Failure to observe the Raman signal corresponding to ammonia and perchloric acid or any other new species in the time-resolved Raman spectra (Figure 4) occurs because the products of reaction 1 are intermediates that are short-lived and engage in further reactions. As a result, the concentration of these intermediates (and any other intermediates that may form) at any instant will remain low. On the other hand, within the submicrosecond time scale of our experiments, the decomposition process will not progress far enough to accumulate a substantial amount of the final decomposition products, Cl_2, O_2, H_2O, N_2O, and so forth. Since the detection system is not sensitive enough to detect low concentrations or weakly scattering molecules, it will not show any new Raman features. However, we can still monitor the depletion of AP as long as the Raman signal exceeds the noise level (Figure 4).

To summarize, our spectroscopic observations are consistent with the proton-transfer reaction widely regarded in the literature as the fundamental step initiating the decomposition of AP under other experimental conditions. However, consistency does not constitute a proof and additional data are required before a more definitive assessment can be made.

V. Summary

Time-resolved Raman and light extinction experiments, along with VISAR particle velocity measurements, were performed on shocked AP single crystals. The Raman modes of AP were monitored under stepwise loading to 10−18 GPa peak stresses. For particular stress and temperature conditions, the intensity of the Raman spectra decayed exponentially. This decay is attributed to shock-induced decomposition in AP. Raman experiments reaching different pressure-temperature states showed that the reaction rate has a positive temperature dependence and a negative pressure dependence over the range of conditions examined here. Results from VISAR particle velocity measurements and light extinction experiments are consistent with the Raman results and confirm that the decay of the Raman peaks is due to chemical decomposition in shocked AP. No orientation dependence was found when AP crystals were shocked normal to the (210) and (001) crystallographic planes. The kinetic and spectroscopic data are consistent with a proton-transfer reaction as the first decomposition step in shocked AP, but our results do not constitute a proof of this mechanism.

Acknowledgment. The authors are grateful to Dr. T. L. Boggs for providing the AP crystals. D. Savage and K. Zimmerman are thanked for their expert assistance in the experimental effort. Dr. B. J. Jensen is acknowledged for executing the VISAR experiments. This work was supported by the Office of Naval Research and the Lawrence Livermore National Laboratory.

References and Notes

(1) Jacobs, P. W. M.; Whitehead, H. M. *Chem. Rev.* **1969**, *69*, 551.

(2) Jacobs, P. W. M.; Pearson, G. S. *Combust. Flame* **1969**, *13*, 419.

(3) Hall, A. R.; Pearson, G. S. *Oxidation and Combust. Revs.* **1968**, *3*, 129.

(4) Yuan, G.; Feng, R.; Gupta, Y. M.; Zimmerman, K. *J. Appl. Phys.* **2000**, *88*, 2371.

(5) Winey, J. M.; Gruzdkov, Y. A.; Dreger, Z. A.; Jensen, B.; Gupta, Y. M. *J. Appl. Phys.* **2002**, *91*, 5650.

(6) Peiris, S. M.; Pangilinan, G. I.; Russell, T. P. *J. Phys. Chem. A* **2000**, *104*, 11188.

(7) Gupta, Y. M. *J. de Physique IV, Colloque C4* **1995**, *5*, C4−345.

(8) Pangilinan, G. I.; Gupta, Y. M. *J. Phys. Chem.* **1994**, *98*, 4522.

(9) Winey, J. M.; Gupta, Y. M. *J. Phys. Chem. B* 1997, *101*, 10733.

(10) Gruzdkov, Y. A.; Gupta, Y. M. *J. Phys. Chem. A* **1998**, *102*, 2322.

(11) Dreger, Z. A.; Gruzdkov, Y. A.; Gupta, Y. M.; Dick, J. J. *J. Phys. Chem. B* **2002**, *106*, 247.

(12) Brill, T. B.; Goetz, F. *J. Chem. Phys.* **1976**, *65*, 1217.

(13) Barker, L. M.; Hollenbach, R. E. *J. Appl. Phys.* **1972**, *43*, 4669.

(14) Sandusky, H. W.; Glancy, B. C.; Carlson, D. W.; Elban, W. L.; Armstrong, R. W. *J. Propulsion and Power* **1991**, *7*, 518.

(15) Elban, W. L.; Sandusky, H. W.; Beard, B. C.; Glancy, B. C. *J. Propulsion and Power* **1995**, *11*, 24.

(16) Fowles, G. R.; Duvall, G. E.; Asay, J.; Bellamy, P.; Feistman, F.; Grady, D.; Michaels, T.; Mitchell, R. *Rev. Sci. Instrum.* **1970**, *41*, 984.

(17) Gupta, Y. M.; Zimmerman, K. A.; Rigg, P. A.; Zaretsky, E. B.; Savage, D.; Bellamy, P. *Rev. Sci. Instrum.* **1999**, *70*, 4008.

(18) Barker, L. M.; Hollenbach, R. E. *J. Appl. Phys.* **1970**, *41*, 4208.

(19) Carter, W. J. *High Temps. − High Pressures* **1973**, 5, 313.

(20) McQueen, R. G.; Marsh, S. P.; Taylor, J. W.; Fritz, J. N.; Carter, W. J. In *High Velocity Impact Phenomena*; Kinslow, R., Ed.; Academic Press: New York, 1970; pp 293−417.

(21) *LASL Shock Hugoniot Data*; Marsh, S. P., Ed.; University of California Press: Berkeley, 1980; p 212.

(22) Jones, S. C.; Gupta, Y. M. *J. Appl. Phys.* **2000**, *88*, 5671.

(23) Schmidt, S. C.; Moore, D. S.; Schiferl, D.; Chatelet, M.; Turner, T. P.; Shaner, J. W.; Shampine, D. L.; Holt, W. T. In *Advances in Chemical Reaction Dynamics, Proc. NATO Advanced Study Institute*; Iraklion, Greece, Rentzepis, P. M., Capellos, C., Eds.; Reidel: Dordrecht, 1986; p 425.

(24) Brill, T. B.; Goetz, F. In *Experimental Diagnostics in Combustion of Solids*; Boggs, T. L., Zinn, B. T., Eds.; American Institute of Aeronautics and Astronautics: New York, 1978; p 3.

(25) Brill, T. B.; Brush, P. J.; Patil, D. G. *Combust. Flame* **1993**, *94*, 70.

(26) Asano, T.; le Noble, W. J. *Chem. Rev.* **1978**, *78*, 407.

(27) Kohnstam, G. *Prog. React. Kinet.* **1970**, *5*, 335.

(28) The estimate of the activation volume, $\Delta V^{\neq}$, was made as follows: $\Delta V^{\neq} = -RT(\Delta \ln k/\Delta p)$, where R is the gas constant, T is temperature, k is the rate constant, and p is pressure. Using the following values of the parameters: $T = 600$ K, $k_1 < 5 \times 10^4$ s^{-1}, $k_2 = 2.1 \times 10^6$ s^{-1}, and $\Delta p = 2.9$ GPa, we find $\Delta V^{\neq} \geq 6.4$ cm^3/mol.

(29) Kraeutle, K. J. *J. Phys. Chem.* **1970**, *74*, 1350.